Coalescence dynamics of viscous conical drops

Jiakai Lu, Shengyang Fang, and Carlos M. Corvalan[*]

Transport Phenomena Laboratory, Department of Food Science, Purdue University, West Lafayette, Indiana 47907, USA

(Received 26 October 2015; published 18 February 2016)

When two oppositely charged drops come into light contact, a liquid meniscus bridge with double-cone geometry forms between the drops. Recent experiments have demonstrated the existence of a critical cone angle above which the meniscus bridge pinches off and the drops do not coalesce. This striking behavior—which has implications for processes ranging from the coarsening of emulsions to electrospray ionization in mass spectrometry—has been studied theoretically and experimentally for inertial liquid drops. Little is known, however, about the influence of the liquid viscosity on the critical cone angle. Here, we use high-fidelity numerical simulations to gain insight into the coalescence dynamics of conical drops at intermediate Reynolds numbers. The simulations, which account for viscous, inertial, and surface tension effects, predict that the critical cone angle increases as the viscosity of the drops decreases. When approaching the inertial regime, however, the predicted critical angle quickly stabilizes at approximately $27°$, as observed in experiments.

I. INTRODUCTION

When two oppositely charged drops in an electric field are sufficiently close, the adjacent interfaces develop a protruding conical shape known as a Taylor cone [1]. As a result, when the drops eventually come into contact the liquid meniscus bridge connecting the drops adopts a double-cone geometry, as sketched in Fig. 1(b). Remarkably, recent experiments by Ristenpart *et al.* [2] have shown that above a critical cone angle β_c the meniscus bridge becomes unstable, and the drops fail to coalesce.

The dynamics of charged drops have important implications for a a wide range of physical processes. Examples include the coalescence of drops in thunderstorms, electrospray ionization in mass spectrometry, oil dehydration, and the coarsening of pH-sensitive emulsions [3–6]. Coalescence of small charged drops also plays an important role in digital microfluidics and in electrodemulsification in microfluidic devices [7,8].

Recently, the noncoalescence dynamics of inertial conical drops have been studied both theoretically and experimentally [2,9–11], and the critical cone angle for low-viscosity drops has been well characterized experimentally [2,9] as $\beta_c = 27° \pm 2°$. However, surprisingly little is known about the noncoalescence dynamics of viscous conical drops. In particular, how viscosity influences the stability of the conical meniscus bridge, and therefore how the critical cone angle changes with the Reynolds number, is still an open question.

Indeed, in a very recent numerical work, Bartlett *et al.* [12] investigated the noncoalescence dynamics of conical drops using a volume-of-fluid technique. Their findings provide important insight into the influence of fluid inertia on the evolution of the conical meniscus bridge. But results from the simulations correspond to nearly inviscid drops. For conditions representative of millimeter water drops these authors predicted a critical angle of $25°$, consistent with the experimental observations by Ristenpart *et al.* [2] and Bird *et al.* [9].

Here, we use high-fidelity numerical simulation to gain insight into the influence of viscosity on the dynamics of conical drops. Results show that increasing the fluid viscosity favors the breakup of the conical meniscus bridge. Accordingly, we find that the critical cone angle characterizing the phase boundary between coalescence and noncoalescence exhibits a strong dependence on the Reynolds number in the viscous regime. Conversely, for low-viscosity drops our simulations predict a constant critical cone angle $\beta_c \approx 27°$, as observed in experiments [2].

II. PROBLEM DESCRIPTION

We consider two supported liquid drops connected by a tiny meniscus bridge at the intersection of two Taylor cones, as shown in Fig. 1. The drops have radius R, density ρ, viscosity μ, and surface tension σ [Fig. 1(a)]. The cone angle is β, and the meniscus bridge has an initial radius R_0 at $z = 0$ [Fig. 1(b)]. The drops are assumed to be sufficiently small that gravity is negligible compared with capillary forces, and the air around the drops is considered dynamically inert.

The dimensionless equations governing the evolution of the liquid velocity $\mathbf{v}$ and the pressure p in the drops, as well as the evolution of the drop interface, are the axisymmetric Navier-Stokes system

$$\nabla \cdot \mathbf{v} = 0, \tag{1}$$

$$\mathrm{Re}\left(\frac{\partial \mathbf{v}}{\partial t} + \mathbf{v} \cdot \nabla \mathbf{v}\right) = \nabla \cdot \mathbf{T} \tag{2}$$

and the kinematic and stress conditions at the fluid surface

$$\mathbf{n} \cdot (\mathbf{v} - \mathbf{v}_s) = 0, \tag{3}$$

$$2\mathcal{H}\,\mathbf{n} = \mathbf{n} \cdot \mathbf{T}. \tag{4}$$

Here $\mathbf{T} = -p\mathbf{I} + (\nabla \mathbf{v} + \nabla \mathbf{v}^T)$ is the stress tensor, $\mathbf{n}$ the outward normal vector, and $\mathbf{v}_s$ the velocity of the surface [13]. The local mean curvature of the interface $\mathcal{H} = (\kappa_r + \kappa_z)/2$ is obtained using the exact expression

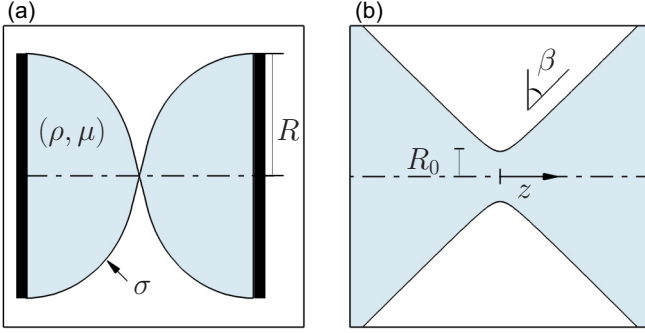$$\mathcal{H} = -1/2(\nabla_s \cdot \mathbf{n}), \tag{5}$$

---
[*]corvalac@purdue.edu

FIG. 1. (a) Sketch of the conical liquid drops and (b) the joining meniscus bridge. The radius of the drops is R, and the cone angle is β. The density of the liquid is ρ, the viscosity is μ, and the surface tension is σ.

where $\nabla_s = (\mathbf{I} - \mathbf{nn}) \cdot \nabla$ is the surface gradient operator [13]. Therefore, the axisymmetric radial and azimuthal curvatures are calculated numerically as

$$\kappa_z = (d\mathbf{t}/ds) \cdot \mathbf{n}, \qquad (6)$$

$$\kappa_r = -(\mathbf{n} \cdot \mathbf{e}_r)/r_s, \qquad (7)$$

where s is the arc length and $\mathbf{t}$ is the unit vector tangent to the interface, following the procedure described in detail by Kistler and Scriven [14]. In this study the length scale is the radius R, the time scale is the viscous time $\tau = \mu R/\sigma$, and the stress scale is the capillary stress σ/R. Therefore, the Reynolds number $\mathrm{Re} = \rho \sigma R/\mu^2$ relates the ratio of inertial to viscous forces with $R/\tau = \sigma/\mu$ as the velocity scale of the fluid. Note that, alternatively, the Reynolds number can be expressed in terms of the Ohnesorge number Oh as $\mathrm{Re} = \mathrm{Oh}^{-2}$, where $\mathrm{Oh} = \mu/\sqrt{\rho \sigma R}$.

The supported drops are axisymmetric about the centerline $r = 0$ and symmetric about the midplane $z = 0$. The initial shape of the interface corresponds to the shape used by Bartlett *et al.* [Eq. (2.1)] [12] to analyze the coalescence dynamics of conical drops of nearly inviscid fluids. Similarly, the initial neck radius $r_0 = R_0/R = 10^{-4}$ and the initial meniscus curvature $\mathcal{H}_0 = 1/2(\kappa_{r0} + \kappa_{z0}) = 1/r_0$, where the initial radial curvature $\kappa_{r0} = -1/r_0$ and the initial azimuthal curvature $\kappa_{z0} = 3/r_0$ were also taken from Bartlett *et al.* [12]. Note that the axial curvature and azimutal curvatures are competing factors that determine the initial breakup or coalescence of the conical drops [15]. As described in detail by Bartlett *et al.* [12], the choice of initial meniscus curvatures in this study leads to a neck region with a positive initial mean curvature $\mathcal{H}_0 = 1/r_0$, resulting in a negative capillary pressure in the neck, which favors coalescence at the beginning. The drops are supported by solid surfaces in which no-slip and no-penetration conditions are imposed and in which the circular contact lines are considered static.

The numerical approach is based on the simultaneous solution of the full Navier-Stokes governing equations using the arbitrary Lagrangian-Eulerian method of spines [14] with an adaptive finite-element mesh and adaptive time integration and a full analytical Jacobian. We have successfully validated and applied this numerical approach to the study of drop
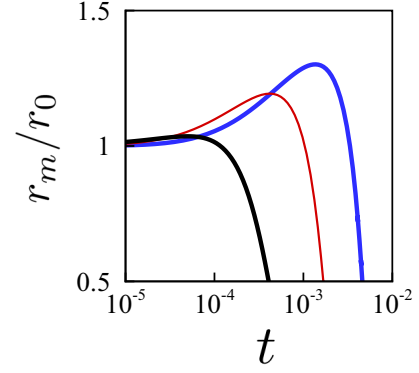

FIG. 2. Radius of the meniscus bridge for three Reynolds numbers. Time evolution of the minimum neck radius r_m for conical drops with cone angle $\beta = 50°$ and three Reynolds numbers: $\mathrm{Re} = 2 \times 10^5$ ($\mathrm{Oh} = 2.2 \times 10^{-3}$) [thick (blue) line], $\mathrm{Re} = 2 \times 10^4$ ($\mathrm{Oh} = 7.07 \times 10^{-3}$) [thin (red) line], and $\mathrm{Re} = 2 \times 10^2$ ($\mathrm{Oh} = 7.07 \times 10^{-2}$) (black line).

coalescence [16] and other free surface flows [17–20] in previous works where more details of the algorithm are given.

III. RESULTS AND DISCUSSION

A. Wide cone angle

Recent experiments have shown that low-viscosity conical drops fail to coalesce if the angle β of the Taylor cone is wider than approximately $27°$ [2]. Thus, we begin our discussion with an example that illustrates the effect of the fluid viscosity on noncoalescing conical drops with a cone angle $\beta > 27°$.

Figure 2 shows the evolution of the minimum radius r_m of the thinning neck for conical drops with a wide cone angle, $\beta = 50°$, and three values of the Reynolds number: $\mathrm{Re} = 2 \times 10^5$ [inertial; thick (blue) line], $\mathrm{Re} = 2 \times 10^4$ [intermediate; thin (red) line], and $\mathrm{Re} = 2 \times 10^2$ [viscous; thick black line]. For the purpose of our discussion, the central observation in Fig. 2 is that increasing the fluid viscosity limits the extent to which the neck can grow before starting to contract.

The liquid neck connecting the inertial drops starts to contract at a minimum neck radius $r_m/r_0 \approx 1.3$, after the capillary pressure jump becomes positive and sufficiently large to drive the fluid away from the neck, as shown in Fig. 3 [thick (blue) line]. The theoretical background of the role of the capillary pressure in the dynamics of inertial conical drops was explained by Bird *et al.* [9] and Helmensdorfer and Topping [10]. The liquid bridge connecting the viscous drops, however, starts to contract at a smaller neck radius $r_m/r_0 \approx 1.036$, long before the pressure becomes positive, as also shown in Fig. 3 (black line). Thus, the contraction is initially driven not by the capillary pressure but, rather, by the enhanced viscous transfer of axial momentum on the viscous drops, as illustrated in Fig. 4.

Figure 4 shows the temporal evolution of the cross-sectional velocity field in the liquid bridge joining the viscous drops. The figure illustrates the significance of the viscous momentum transfer at the incipience of the transition from coalescence to noncoalescence. In the online version, the red area indicates positive radial flow (flow away from the symmetry axis) and
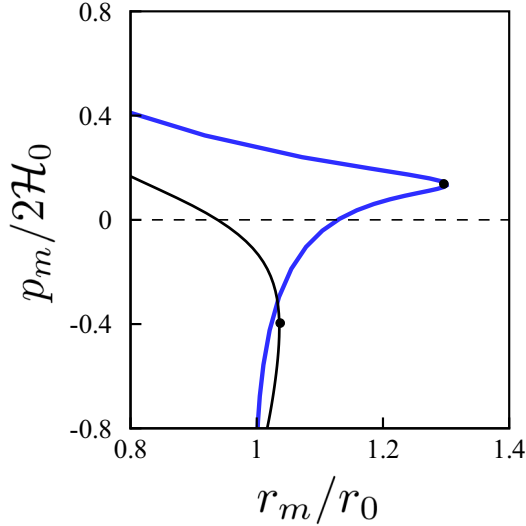
FIG. 3. Evolution of the pressure on the meniscus bridge for two Reynolds numbers. Evolution of the capillary pressure on the meniscus bridge p_m for conical drops with cone angle $\beta = 50°$ and Reynolds numbers Re $= 2 \times 10^5$ (Oh $= 2.2 \times 10^{-3}$) [thick (blue) line] and Re $= 2 \times 10^2$ (Oh $= 7.07 \times 10^{-2}$) (black line).

the blue area indicates negative radial flow (flow toward the axis). Figure 4(a) shows that during the coalescence phase the negative capillary pressure induced by the meniscus curvature drives a positive radial flow on the meniscus bridge that expands the neck radius (red area in the figure). As time progresses, the viscous transfer of momentum from the region on the conical side of the drops with a negative radial velocity [blue area in Fig. 4(b)] decelerates and gradually reverses the growth of the meniscus neck, which was initially moving with a positive radial velocity. Finally, Fig. 4(c) illustrates the reversal of the original flow pattern at the meniscus interface. Here, the full meniscus interface starts to move towards the axis of symmetry, revealing the beginning of the noncoalescence process. This reversal corresponds to the maximum of the r_m in Fig. 3 (black line) and therefore occurs despite the capillary pressure being negative at the neck. Only after the neck radius decreases below $r_m \approx 9.3 \times 10^{-5}$ does the capillary pressure
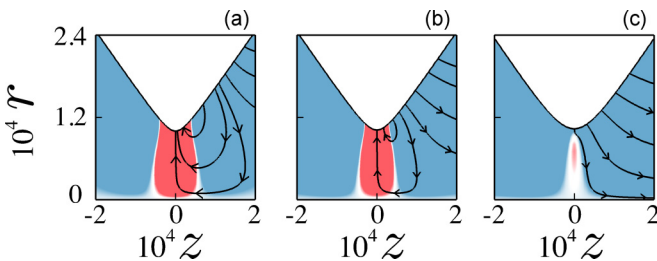

FIG. 4. Velocity field in the conical meniscus bridge. Evolution of the radial velocity field in the meniscus bridge for conical viscous drops with Re $= 2 \times 10^2$ (Oh $= 7.07 \times 10^{-2}$) and cone angle $\beta = 50°$ at dimensionless times $t = 0.1 \times 10^{-5}, 1.3 \times 10^{-5}$, and 5.4×10^{-5} (left to right). Here red corresponds to positive radial velocity and blue to negative radial velocity.
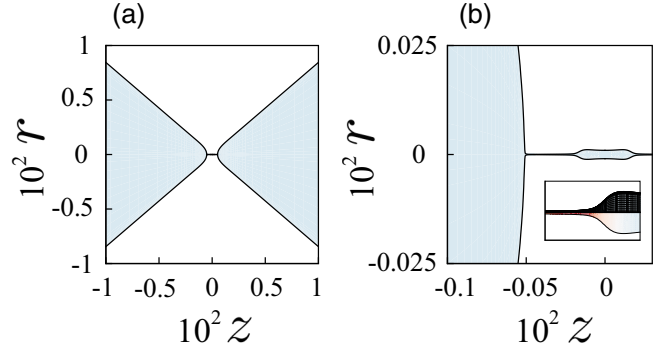

FIG. 5. Interface shape of a conical meniscus bridge near pinch-off. (a) Interface shape of the conical meniscus bridge formed between two conical drops with Re $= 2 \times 10^4$ (Oh $= 7.07 \times 10^{-3}$) and $\beta = 50°$ when the minimum neck radius is $r_m = 5 \times 10^{-7}$. (b) Magnified view of the satellite droplet formed in the filament connecting the main drops.

become positive and contribute to the thinning of the liquid bridge.

The above results show that the viscous momentum transfer has a destabilizing effect on the conical meniscus bridge and, thus, suggest that narrower cone angles, $\beta < 27°$, exist, for which inertial drops will coalesce but viscous drops may still fail to coalesce. But before moving on to show, in Sec. III C, that such opening angles do indeed exist, we pause to note that the pinch-off dynamics follow scalings and self-similarities at the imminence of breakup that have been well established theoretically and that can be used as a stringent benchmark.

B. Scaling and self-similarity

Different shapes and scalings were observed during the pinch-off of the drops in Fig. 2, depending on whether inertia or viscosity was dominant in the dynamics. For example, a small satellite drop was observed between the inertial drops (Re $= 2 \times 10^5$) but no satellite drop was observed during the pinch-off of the high-viscosity drops (Re $= 2 \times 10^2$). In this section, we describe the shape and the self-similar behavior observed for the drops with the intermediate Reynolds number Re $= 2 \times 10^4$. We focus on the drops with intermediate Re because they successively exhibit both inertial and viscous behavior while approaching the singularity.

Figure 5(a) illustrates the interfacial shape of the liquid bridge at the imminence of breakup ($r_m \approx 5 \times 10^{-7}$) for the conical drops with Re $= 2 \times 10^4$. The enlarged view in Fig. 5(b) makes clear that a small satellite droplet has formed between the main drops, as typically observed during the breakup of moderately viscous liquid filaments due to the Rayleigh instability [21]. In addition, Fig. 6 demonstrates that both the temporal and the spatial coalescence dynamics exhibit self-similar behavior near breakup. Figure 6(a) shows that the minimum radius of the thinning neck r_m versus the time to collapse t' initially exhibits the 2/3 scaling that can be expected from straightforward dimensional analysis of the inertial limit [22] (dashed line). As the neck radius decreases, however, local viscous effects become dominant and the temporal scaling merges onto Eggers' viscous universal solution,
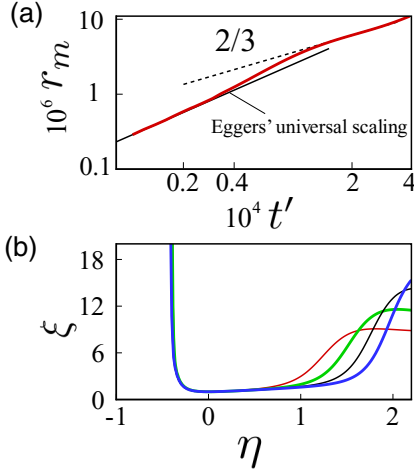
FIG. 6. Scaling and self-similarity. (a) Evolution of the thinning neck radius r_m with the time to pinch-off $t' = t - t_0$, where t_0 is the time of pinch-off, for conical drops with $\beta = 50°$ and $\mathrm{Re} = 2 \times 10^4$ ($\mathrm{Oh} = 7.07 \times 10^{-3}$). The radius initially follows a 2/3 power-law scaling (dashed line) and then transitions to Eggers' universal scaling $r_m = 0.0304 t'$ (solid black line). (b) Interface shapes in similarity coordinates $\xi = r/r_m$ and $\eta = t'^{0.5}(z - z_m)/r_m$ for neck radius $r_m = 1.004 \times 10^{-6}$ [thin (red) line], 8.215×10^{-7} [thick (green) line], 6.785×10^{-7} (black line), and 5.077×10^{-7} [thick (blue) line].

$r_m = 0.0304 \ t'$ (black line) [23]. Due to the orders-of-magnitude gap between the initial neck radius r_0 and the minimum neck radius r_m, the drop profile also exhibits spatial self-similarity near the singularity [21]. This is illustrated in Fig. 6(b), which shows that the portion of the interface over which the neck profiles approach a similar shape increases as r_m goes to zero when plotted in scaled similarity coordinates $\xi = r/r_m$ and $\eta = t'^{0.5}(z - z_m)/r_m$, where z_m is the axial coordinate of the minimum neck radius.

C. Phase diagram showing regions of coalescence and breakup

In Sec. III A we discuss the destabilizing influence of the viscosity for conical drops with cone angle $\beta > 27°$. Here, we show that this destabilizing influence can prevent the coalescence of conical drops with cone angles $\beta < 27°$ and, consequently, modifies the phase boundary between coalescence and noncoalescence.

This is first exemplified in Fig. 7. In the figure, we compare the time evolution of the minimum neck radius r_m for three conical drops with intermediate Reynolds number $\mathrm{Re} = 2 \times 10^4$ and three values of the cone angle: $\beta = 22°$ [thick (blue) line], $\beta = 23°$ (black line), and $\beta = 25°$ [thin (red) line]. For the parameters used in the figure, the simulations predict that the transition between coalescence and noncoalescence occurs for a critical cone angle $22° < \beta_c < 23°$, a few degrees smaller than the critical cone angle $\beta_c \approx 27°$ corresponding to inertial drops.

We have performed a number of similar simulations to map the regions of coalescence and noncoalescence spanning about three orders of magnitude in the Reynolds number. We focus on characterizing the influence of the Reynolds number, so the other parameters are held constant. The resulting diagram
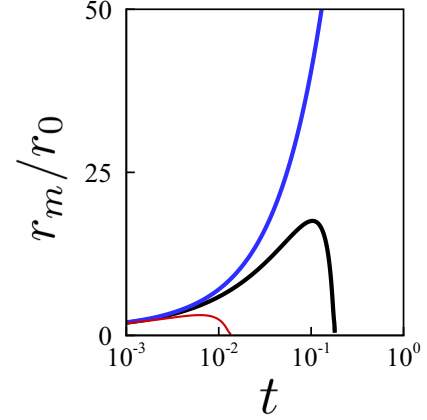

FIG. 7. Radius of the meniscus bridge for three cone angles. Time evolution of the minimum neck radius r_m for conical drops with $\mathrm{Re} = 2 \times 10^4$ ($\mathrm{Oh} = 7.07 \times 10^{-3}$) and cone angles $\beta = 22°$ [thick (blue) line], $\beta = 23°$ (thick black line), and $\beta = 25°$ [thin (red) line].

demonstrates, for the first time, to our knowledge, that the phase boundary between coalescence and noncoalescence exhibits a strong dependence on the Reynolds number (Fig. 8). Specifically, we find that the boundary between coalescence and noncoalescence is characterized by a critical cone angle β_c that increases with the Reynolds number (Fig. 8; filled symbols). We note that, as the Reynolds number decreases and the characteristic viscous length scale becomes increasingly large, the influence of the macroscopic drop configuration (e.g., supported as opposed to freestanding drops) should become more relevant. The results in Fig. 8, however, correspond to drops with $\mathrm{Re} = \rho \sigma R / \mu^2 \gg 1$—that is, drops with a radius R much larger than the viscous length scale $l_\mu = \mu^2 / \rho \sigma$— which are expected to be largely insensitive to macroscopic changes in configuration. We have tested this expectation at
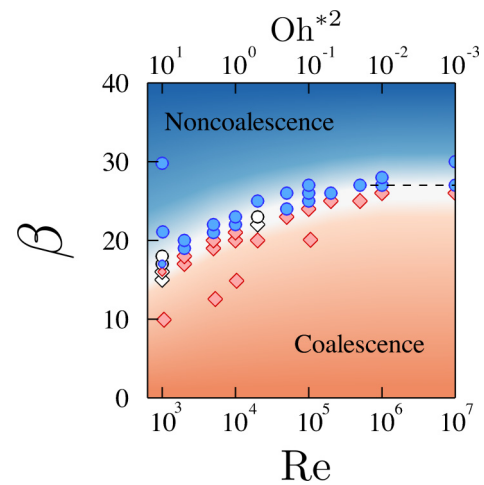

FIG. 8. Phase diagram showing regions of coalescence and noncoalescence. Instances of coalescence [(red) diamonds] and noncoalescence [(blue) circles] in the Re and β space for conical drops with $r_0 = 10^{-4}$ and $\mathcal{H}_0 = 10^4$. Filled symbols correspond to supported drops, and open symbols correspond to freestanding drops. Here, $\mathrm{Oh}^* = \mu/\sqrt{\rho \sigma R_0}$ is the local Ohnesorge number based on the neck radius.

the lower end of the Reynolds numbers in Fig. 8. We performed simulations for Re $= 1 \times 10^3$ and Re $= 2 \times 10^4$ for the more computationally demanding freestanding drops, and the results are depicted as open symbols in Fig. 8. The simulations show no differences between the critical cone angle of the supported and that of the freestanding drops. We have also tested the influence of the initial meniscus shape by decreasing the radius of the initial meniscus curvature up to a full order of magnitude smaller and found no differences in the predicted critical cone angles.

In addition, the phase diagram shows that as the Reynolds number increases and viscous effects become negligible, the critical cone angle rapidly stabilizes and then remains essentially constant. Therefore, it is relevant to compare the results in this region with the experimental measurement of the critical cone angle of inertial drops by Ristenpart *et al.* [2] and Bird *et al.* [9]. In this regard, the results from our full N-S simulations predict that the inertial cone angle in the region of large Reynolds numbers is $\beta_c \approx 27°$ (Fig. 8; dashed line), in excellent agreement with the value $\beta_c = 27° \pm 2°$ observed in the experiments.

IV. CONCLUSION

In this work, we have studied the noncoalescence dynamics of viscous conical drops using direct numerical simulations. We have demonstrated that this approach is highly accurate,

as it is able to reproduce asymptotic self-similar behavior at the imminence of the pinch-off of the conical meniscus bridge, including Eggers's universal scaling.

Results from the simulations show that increasing the fluid viscosity favors the pinch-off of the liquid meniscus bridge. Accordingly, results show that the critical cone angle β_c, which characterizes the phase boundary between coalescence and noncoalescence, decreases as the viscosity increases. The nature of the noncoalescence dynamics also changes with the fluid viscosity. While the pinch-off of inertial conical drops is largely due to the higher capillary pressure in the meniscus bridge, which drives the fluid away from the neck [2,9,10], the pinch-off of viscous conical drops is favored by the enhanced transfer of the viscous momentum. Results also show that when the Reynolds number is large and so the characteristic viscous length is negligible, the momentum transfer is ineffective and the critical cone angle becomes constant. Under these conditions, the predicted critical cone angle is $\beta_c \approx 27°$, in excellent agreement with previous experiments on inertial conical drops. We expect that our findings will motivate similar experimental studies on conical drops with lower Reynolds numbers.

[1] G. Taylor, in *Proceedings of the Royal Society of London A: Mathematical, Physical and Engineering Sciences* (The Royal Society, London, 1964), Vol. 280, pp. 383–397.

[2] W. D. Ristenpart, J. Bird, A. Belmonte, F. Dollar, and H. Stone, Nature **461**, 377 (2009).

[3] J. Latham, Rep. Prog. Phys. **32**, 69 (1969).

[4] P. Brazier-Smith, S. Jennings, and J. Latham, in *Proceedings of the Royal Society of London A: Mathematical, Physical and Engineering Sciences* (The Royal Society, London, 1972), Vol. 326, pp. 393–408.

[5] J. S. Eow, M. Ghadiri, A. O. Sharif, and T. J. Williams, Chem. Eng. J. **84**, 173 (2001).

[6] T. Liu, S. Seiffert, J. Thiele, A. R. Abate, D. A. Weitz, and W. Richtering, Proc. Natl. Acad. Sci. USA **109**, 384 (2012).

[7] A. R. Thiam, N. Bremond, and J. Bibette, Phys. Rev. Lett. **102**, 188304 (2009).

[8] D. J. Im, Korean J. Chem. Eng. **32**, 1001 (2015).

[9] J. C. Bird, W. D. Ristenpart, A. Belmonte, and H. A. Stone, Phys. Rev. Lett. **103**, 164502 (2009).

[10] S. Helmensdorfer and P. Topping, Europhys. Lett. **104**, 34001 (2013).

[11] B.-B. Wang, X.-D. Wang, W.-M. Yan, and T.-H. Wang, Langmuir **31**, 7457 (2015).

[12] C. T. Bartlett, G. A. Généro, and J. C. Bird, J. Fluid Mech. **763**, 369 (2015).

[13] J. C. Slattery, *Interfacial Transport Phenomena* (Springer, New York, 1990).

[14] S. F. Kistler and L. E. Scriven, *Coating Flow: Computational Analysis of Polymer Processing* (Applied Science, New York, 1983).

[15] S. Quan, D. P. Schmidt, J. Hua, and J. Lou, J. Fluid Mech. **640**, 235 (2009).

[16] J. Lu and C. M. Corvalan, Chem. Eng. Sci. **78**, 9 (2012).

[17] R. J. Muddu, J. Lu, P. E. Sojka, and C. M. Corvalan, Chem. Eng. Sci. **69**, 602 (2012).

[18] J. Lu and C. M. Corvalan, Chem. Eng. Sci. **119**, 182 (2014).

[19] J. Lu and C. M. Corvalan, Chem. Eng. Sci. **132**, 93 (2015).

[20] J. Lu, J. Yu, and C. M. Corvalan, Langmuir **31**, 8618 (2015).

[21] J. R. Lister and H. A. Stone, Phys. Fluids (1994–present) **10**, 2758 (1998).

[22] R. F. Day, E. J. Hinch, and J. R. Lister, Phys. Rev. Lett. **80**, 704 (1998).

[23] J. Eggers, Phys. Rev. Lett. **71**, 3458 (1993).